



Article

An Experimental Investigation of FRCC Shear Walls Reinforced with Steel and GFRP Bars

Mohammad J. Tolou Kian, Sina Ghazizadeh and Carlos A. Cruz Noguez *

Department of Civil and Environmental Engineering, University of Alberta, Edmonton, AB T6G 2R3, Canada; toloukia@ualberta.ca (M.J.T.K.); ghazizad@ualberta.ca (S.G.)

* Correspondence: cruznogu@ualberta.ca; Tel.: +1-780-492-2794

Received: 12 July 2018; Accepted: 5 September 2018; Published: 10 September 2018



Abstract: Contemporary structures can resist earthquakes as they deform and dissipate energy. However, during strong ground motions, these structures can sustain significant concrete damage and overall permanent deformations. Therefore, it is of great benefit if earthquake-resisting structures can deform and dissipate energy, and yet sustain mitigated damage. This paper illustrates the findings of an experimental study focused on the mitigation of damage and reduction of residual displacements in reinforced concrete (RC) shear walls. In this study, the cyclic properties of two innovative shear walls—a slender and a squat wall—which were cast with fiber-reinforced cementitious composites and reinforced with steel and glass fiber reinforced polymer bars are investigated. Then, the improvements of the innovative specimens with respect to two conventional RC shear walls are discussed in terms of damage propagation, self-centering, stiffness retention and energy dissipation. As the experiments showed, the innovative walls sustained mitigated concrete damage and less residual drift ratios while illustrating significant stiffness and energy dissipation capacities.

Keywords: reinforced concrete (RC); shear wall; damage mitigation; glass fiber reinforced polymer (GFRP); fiber reinforced cementitious composite (FRCC)

1. Introduction

Fiber reinforced polymer (FRP) is a material composed of a polymeric matrix reinforced with fibers of aramid, carbon or glass. Since FRP has a superior strength-to-weight ratio and high durability characteristics with respect to conventional steel, it has been considered as an alternative material in the construction and retrofitting of reinforced concrete (RC) structures. FRP is manufactured in different forms. FRP sheets are usually used in the flexural and shear retrofitting of RC structures when the sheets are used parallel or perpendicular to the direction of vulnerable RC elements [1].

FRP bars are also used to reinforce concrete members in longitudinal or transverse directions. Mohamed et al. [2] studied the response of 14 full-scale circular columns which were reinforced with longitudinal and transverse FRP bars. The longitudinal FRP bars of the specimens were able to resist compression even after the concrete of those specimens had crushed. The transverse FRP reinforcement of each column was able to adequately prevent the buckling of the longitudinal bars. The transverse FRP reinforcement was also able to confine the core of the column specimens even after the peak load of each column was reached. In the case of shear walls, Mohamed et al. [3] studied the in-plane response of four cantilever specimens which had an axial load ratio of 7%. The study included the testing of one steel-reinforced specimen and three fully glass fiber reinforced polymer (GFRP) reinforced concrete shear walls. The GFRP-reinforced walls illustrated satisfactory levels of deformability and more substantial self-centering properties in comparison to the steel-reinforced shear wall of the study. On the other hand, due to the linear behavior of GFRP bars, the GFRP-reinforced walls dissipated less

energy in comparison to the steel reinforced wall. To improve the energy dissipation capacity and promote ductility of FRP-reinforced walls, Ghazizadeh and Cruz-Noguez [4] suggested using hybrid FRP-steel flexural reinforcing systems. Ghazizadeh et al. [5] also conducted a numerical study on squat GFRP-steel reinforced walls showing that the seismic performance of an appropriately designed hybrid FRP-steel reinforced specimen was comparable to RC members in terms of displacement and energy dissipation, while displaying better self-centering behavior. Similar conclusions were drawn from the study by Cai et al. [6], investigating the response of four hybrid columns reinforced with carbon fiber reinforced polymer and steel.

Also, it has been shown through several experimental studies that structural members cast with fiber-reinforced cementitious composites (FRCC) sustain mitigated damage in comparison to conventional RC members. In this regard, Parra-Montesinos and Kim [7] studied the response of two RC shear walls cast with FRCC incorporating polyethylene or hooked-end steel fiber with volume fractions of 1.5% and 2% respectively. The walls were designed to have a diagonal tension failure as they had inadequate web reinforcement. The test results showed that FRCC shear walls had excellent damage resilience and displacement capacities.

To further mitigate damage in RC shear walls, this paper investigates the response of two hybrid shear walls cast with FRCC and reinforced with steel and GFRP bars. Improvement in the resilience of the hybrid walls is illustrated through comparison with two conventional steel-reinforced concrete shear walls subjected to similar displacement demands.

2. Materials and Methods

2.1. Materials

The specimens of this study were comprised of reinforcing bars and cement-based composites. The reinforcing bars used in the construction of specimens were 10M and 15M mild steel bars (McNish Steel and Harris Steel, Edmonton, AB, Canada) with nominal cross-sectional areas of 100 mm² and 200 mm², and #5 and #6 GFRP bars (BP Composites Ltd., Edmonton, AB, Canada), which had nominal cross-sectional areas of 199 mm² and 284 mm² respectively.

The mechanical properties of steel rebars were determined in accordance with the American Society of Testing Materials (ASTM) A370-14 [8]. The 10M and 15M steel bars had an average Young's modulus of 180 GPa, yield strength of 417 MPa and ultimate strength of 634 MPa. The properties of the GFRP bars used were provided by the manufacturer of the bars. As provided, #5 GFRP bars had an elastic behavior with an elasticity modulus of 62.6 GPa corresponding to an ultimate strain of 2.1% and an ultimate stress of 1150 MPa. #6 GFRP bars had a Young's modulus of 62.7 GPa, an ultimate strain of 2.0%, and an ultimate stress of 1150 MPa. Figure 1a,b shows a 10M steel rebar and #5 GFRP bar, and the stress-strain relationships of the mild steel and GFRP bars are illustrated in Figure 1c.

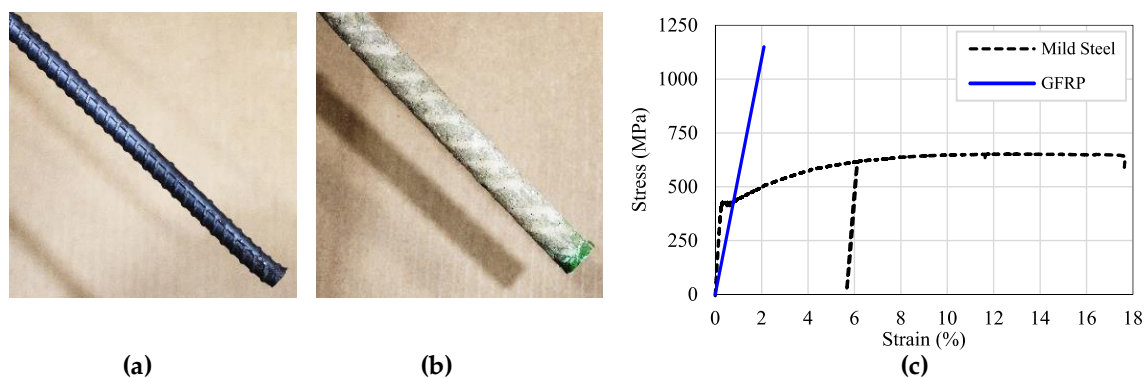


Figure 1. (a) A 10M steel bar; (b) A #5 GFRP bar; (c) Tensile stress-strain relationships of the #5 GFRP bar versus the 10M steel bar.

Two types of cementitious composites were used in this study. The control slender and squat walls were cast with normal concrete mixes that had a maximum aggregate size of 10 mm and compressive strengths of 48 MPa and 61 MPa, which were determined according to ASTM C39-15a [9]. The companion GFRP-reinforced specimens were cast with fiber reinforced composites consisted of engineered cementitious composite (ECC) for the slender wall and steel fiber reinforced concrete (SFRC) for the squat wall, with fiber volume fractions of 2%, and 1.5% respectively. ECC incorporated poly vinyl alcohol fibers (Kuraray, Tokyo, Japan) with a length of 12 mm, while the hooked-end steel fibers (Optimet Concrete Products Inc., Markham, ON, Canada) used in SFRC were 50 mm long. The ECC mix contained no coarse aggregate, while the SFRC mix coarse contained aggregates with a maximum dimension of 10 mm. The ECC was provided by FiberMatrix Inc. (Sparks, NV, USA) and the SFRC by Lafarge (Edmonton, AB, Canada). The ECC and SFRC mixes had compressive strengths of 38.0 MPa and 60.5 MPa. The ultimate compressive strains of the ECC and SFRC cylinders were approximately 2.0% and 1.3% respectively, while it was 0.4% for plain concrete cylinders.

2.2. Test Specimens

Each specimen was comprised of three segments, a foundation, a wall panel and a cap-beam, which were cast monolithically. The specimens were tested as cantilevers in a fixed-free fashion. The foundation of each was anchored to the strong floor of the laboratory while its cap-beam was connected to an actuator, which was used to apply displacement reversals. The out-of-plane displacement component at the top-point of each specimen was restricted as shown in Figure 2.

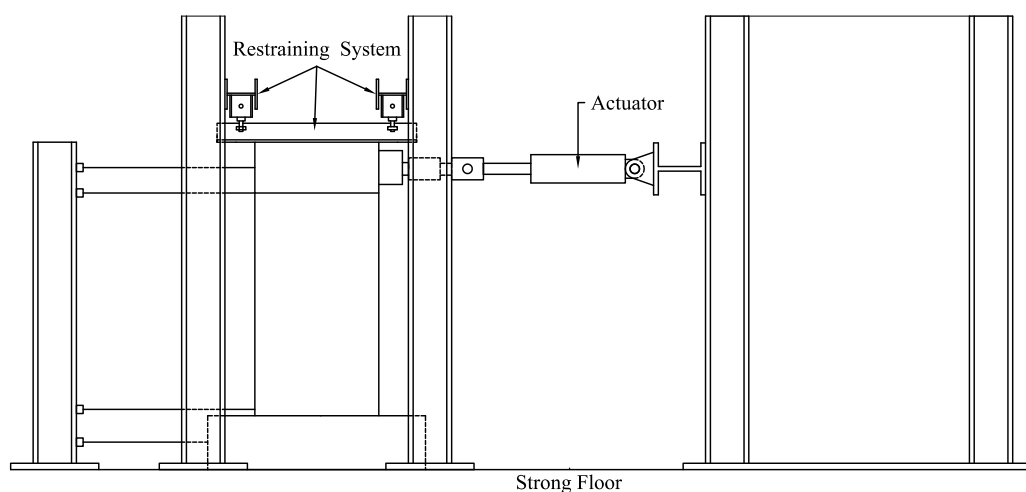


Figure 2. Test setup.

Four specimens, consisting of two slender and two squat walls, were tested in this study. As shown in Figure 3, the slender walls were 1800 mm high, 1000 mm wide, and 150 mm thick with an aspect ratio (shear span to length) of 2.0—the minimum ratio for considering a wall slender according to the Canadian Standards Association (CSA) A23.3-14 [10]. The squat walls had the same height and thickness as the slender walls but a length of 1800 mm, leading to square wall panels with a shear span to length ratio of 1.1.

The two specimens which were cast with conventional concrete and reinforced with steel bars were termed control walls, while the specimens cast with FRCC and reinforced with steel and GFRP bars were termed hybrid walls. All the specimens were designed according to CSA A23.3-14, while hybrid specimens were compliant to CSA S806-12 [11] as well. The hybrid walls were designed to have improved self-centering properties with respect to their corresponding control walls while exhibiting comparable levels of ductility. For this reason, the GFRP bars were placed in the webs of the hybrid specimens and the steel bars were placed within their boundary elements.

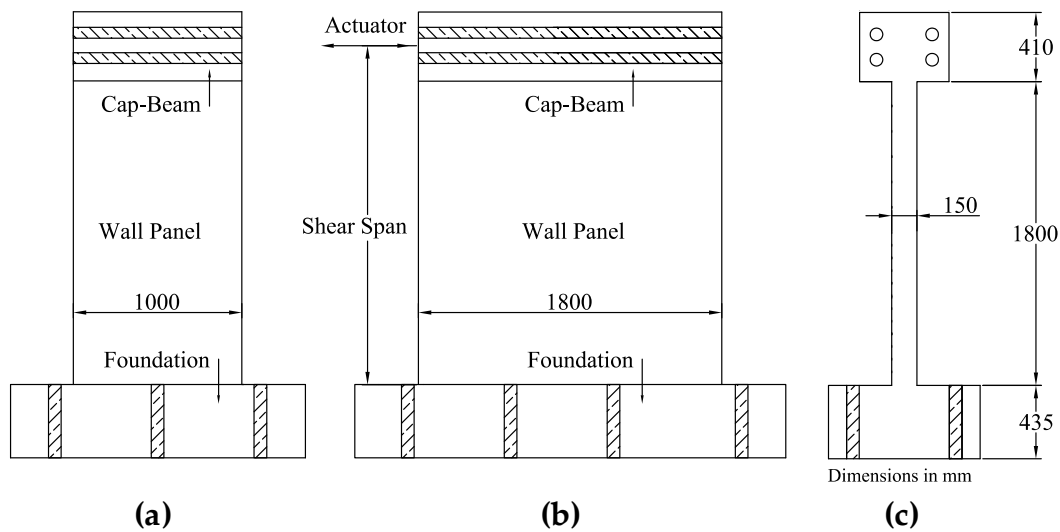


Figure 3. Geometrical properties of test specimens (a) slender walls, front-view; (b) squat walls, front-view; (c) slender and squat walls, side-view.

In the case of the hybrid slender wall, it was decided to maintain the same reinforcing as that of the control slender wall, while substituting some of the web reinforcement of the wall with GFRP bars. The cross-sectional area of the GFRP bars was determined to provide the specimen with maximum self-centering, while also increasing the lateral load resistance of the wall. As a result, #5 GFRP bars were selected to be used since the bars had the largest diameter which was in accordance to the allowable clear spacing between GFRP bars as per CSA S806-12. Figure 4 shows the reinforcement layout of the control and hybrid slender walls.

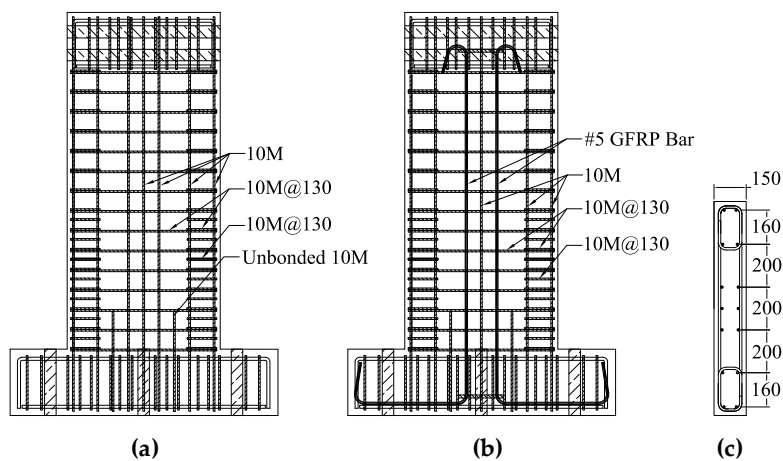


Figure 4. Reinforcement details of (a) the control slender wall, front-view; (b) the hybrid slender wall, front-view; (c) the control and hybrid slender walls, cross-section.

On the other hand, the hybrid squat wall was designed to have a comparable lateral strength to that of the control squat wall. For this reason, instead of 15M bars, used in the control squat wall, 10M bars were used in the construction of the hybrid squat wall to compensate for the over-strength exerted on the specimen by detailing it with #6 GFRP bars. Figure 5 shows the reinforcement layout of the squat walls.

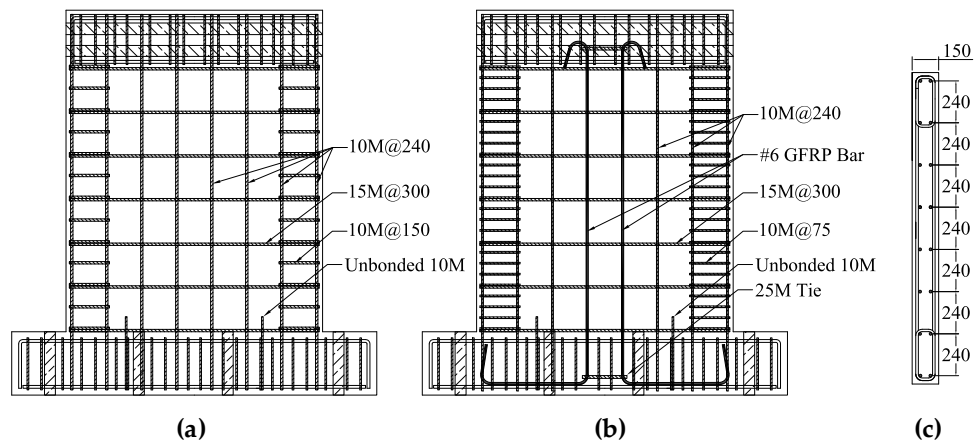


Figure 5. Reinforcement details of (a) the control squat wall, front-view; (b) the hybrid squat wall, front-view; (c) the control and hybrid squat walls, cross-section.

3. Results

3.1. Damage Propagation

Figure 6 shows damaged states of the control slender wall at drift ratios of 0.9%, 1.8%, 2.3% and 4%. It can be seen that the wall formed horizontal and diagonal cracks along its lower heights. Then the concrete cover of the wall started to spall at a drift ratio of 2.7% and suffered more damage towards the end of testing. Finally, the failure of the specimen was triggered by the rupture of two rebars, after the wall had undertaken a demand of 3.3%, which caused a strength degradation of 20%.

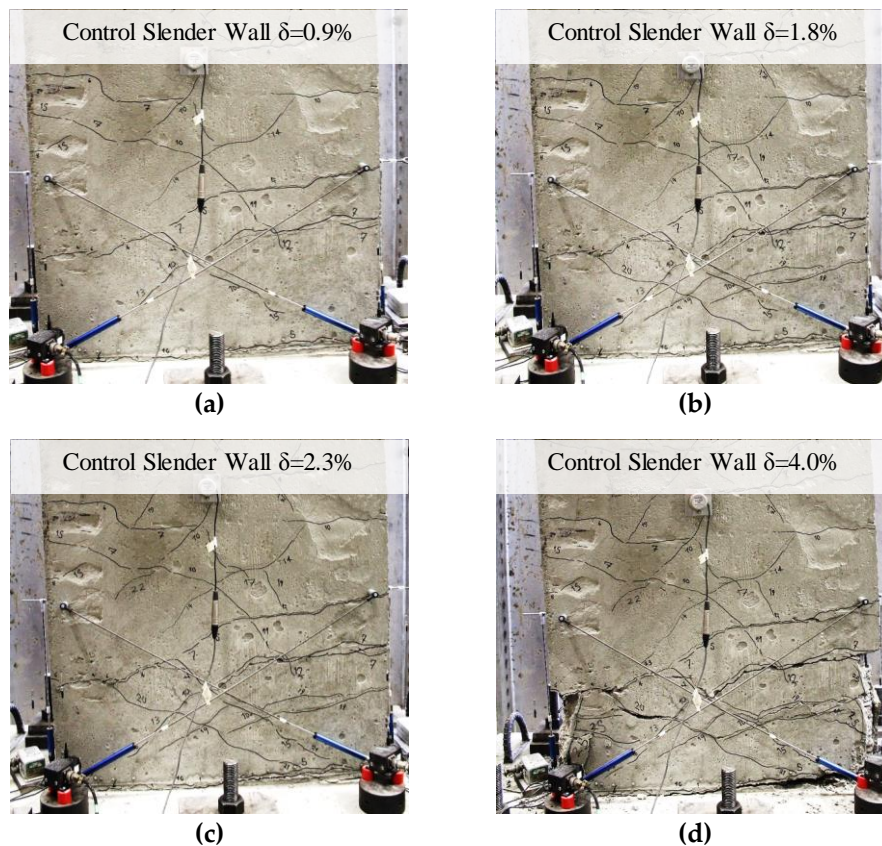


Figure 6. Damage propagation in the control slender wall.

Figure 7 shows damaged states of the hybrid slender wall at drift ratios of 0.9%, 1.8%, 2.3% and 4%. It can be seen that the ECC wall exhibited substantially less damage in terms of concrete cracking and cover spalling in comparison to the control slender wall. As is clear from Figure 7, the specimen formed only a few flexural cracks, with the crack formed at the foundation interface of the wall being the dominant. No spalling was observed during testing of the wall. The specimen underwent rebar failure just before a drift ratio of 3.3%, which initiated the strength degradation of the specimen.

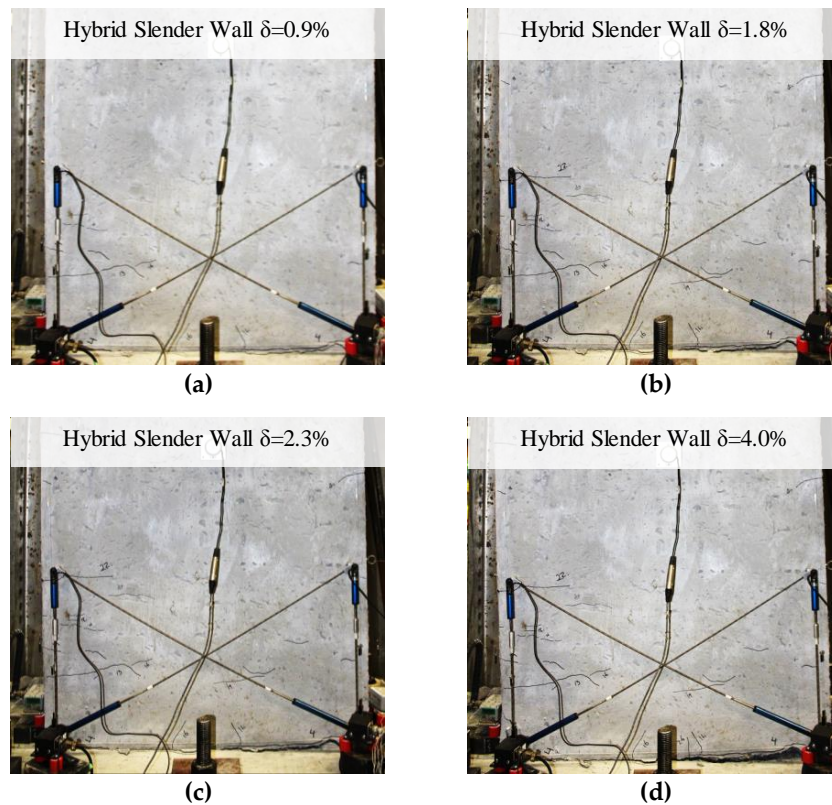


Figure 7. Damage propagation in the hybrid slender wall.

Figure 8 shows the damaged states of the control squat wall at drift ratios of 0.9%, 1.6% and 2.3%. As can be seen in Figure 8, diagonal cracks were distributed more evenly along the height of the specimen in comparison to the slender wall control wall. The concrete cover of the specimen started to spall at a drift ratio of 1.5%, which worsened towards the end of testing. Finally, the failure of the specimen was facilitated by the buckling of the outermost rebars of the wall at 2.2% drift, followed by concrete crushing at the toes of the specimen.

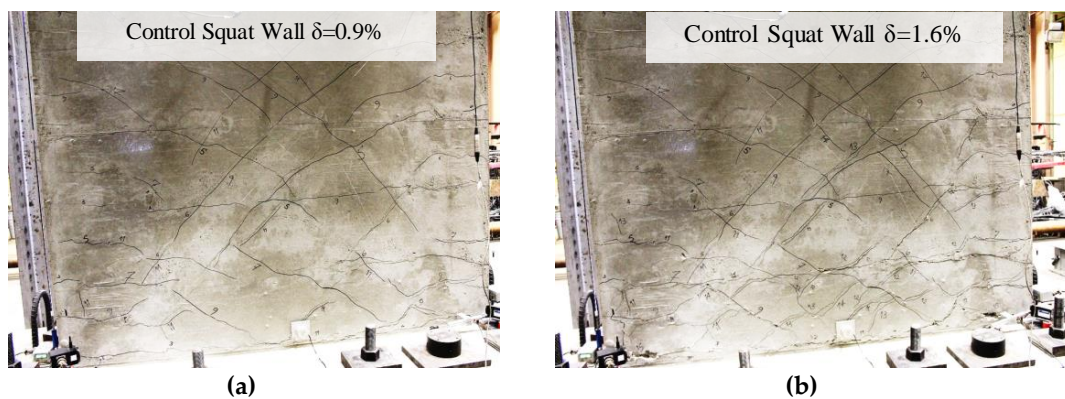


Figure 8. Cont.

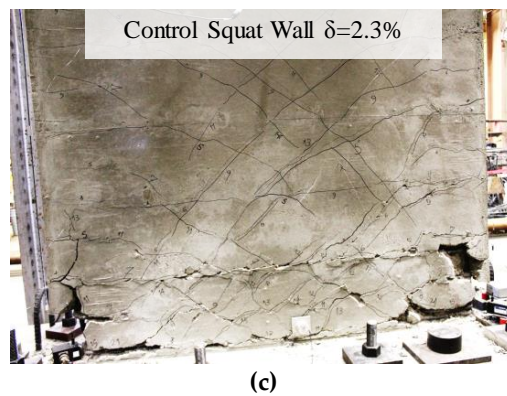


Figure 8. Damage propagation in the control squat wall.

Figure 9 shows damaged states of the hybrid squat wall at drift ratios of 0.9%, 1.6% and 2.3%. Similar to the control squat wall, the specimen formed distributed diagonal cracks along its height. The specimen also underwent spalling at a drift ratio of 1.5%, although less significantly in comparison to the control squat wall. Finally, the strength degradation of the specimen was started by the rupture of outmost rebars of the wall at a drift ratio of -2.0% .

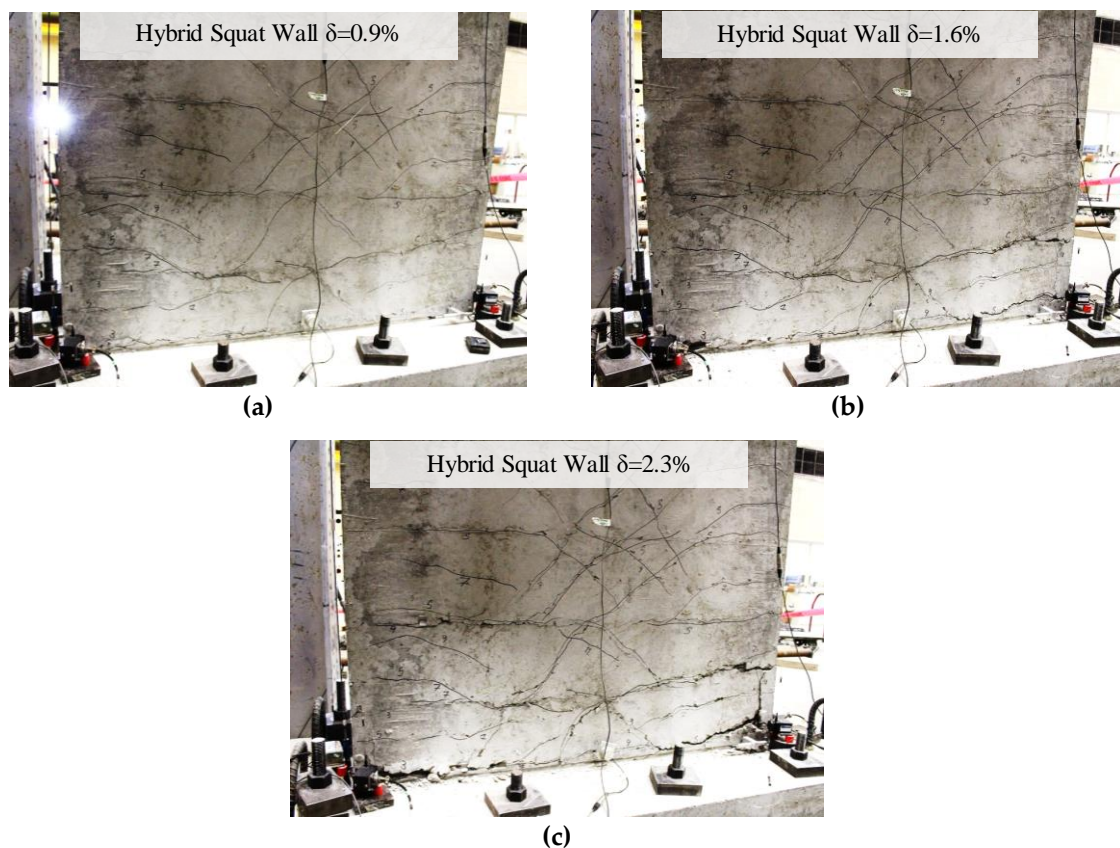


Figure 9. Damage propagation in the hybrid squat wall.

Figure 10 illustrates longitudinal strain distribution on the surface of each wall specimen measured by a digital image correlation (DIC) system at a drift ratio of 2.3%. The locations of cracks on the surface of the wall panels are associated with relatively higher longitudinal strains. According to Figure 10, the control slender and squat walls suffered more significant cracking and spalling above their base. Concrete damage was less significant yet more distributed in the case of hybrid walls.

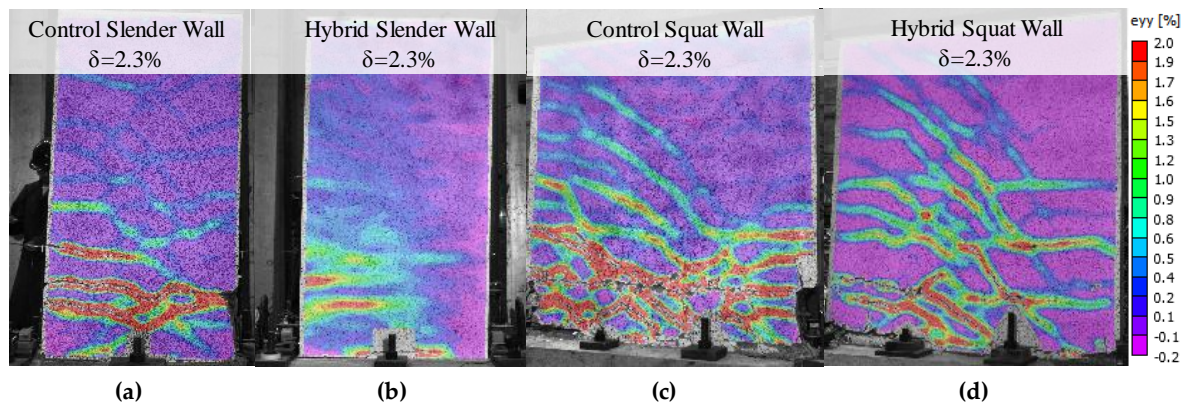


Figure 10. Longitudinal strain distribution of each of specimens at of 2.3% drift.

3.2. Hysteretic Response

The response of each specimen was measured by cable horizontal transducers and a DIC system, as shown in Figure 11. As can be seen in Figure 11, the lateral displacements measured by the DIC system were well in agreement with those of the cable transducers. The relative error between the DIC and the transducer measurements was below 5% for drift ratios of 1.0% and greater.

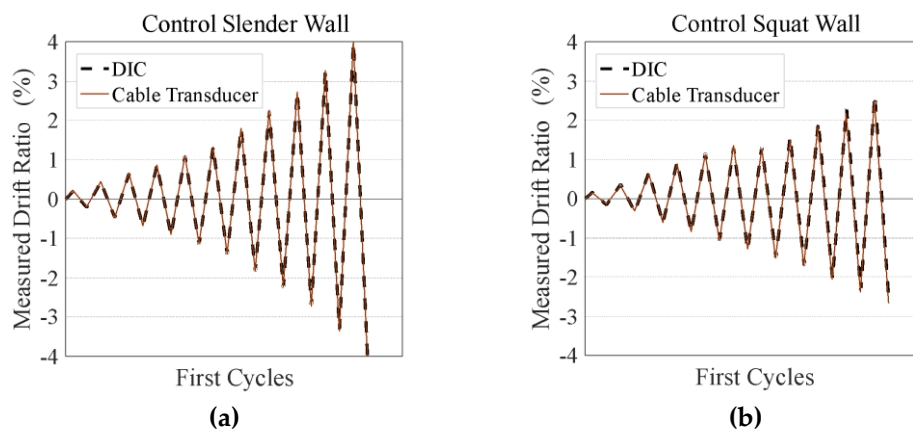


Figure 11. Drift ratios of the control slender and squat walls measured by cable transducers and the DIC system.

The data recorded by the DIC system was of great use, as the system captured horizontal and vertical displacements along the height of each specimen. The data was used to determine the shear and flexural strain distributions and the shear and flexural displacement components along the height of each wall. Figure 12 shows the distribution of average shear strains along the height of each specimen, determined based on the changes in the lengths of two diagonals [12]. According to Figure 12, the squat walls experienced greater and more distributed average shear strains along their heights in comparison to the slender walls. Also, the hybrid walls, which were cast with fiber-reinforced concrete exhibited less shear strains in comparison to their corresponding control walls.

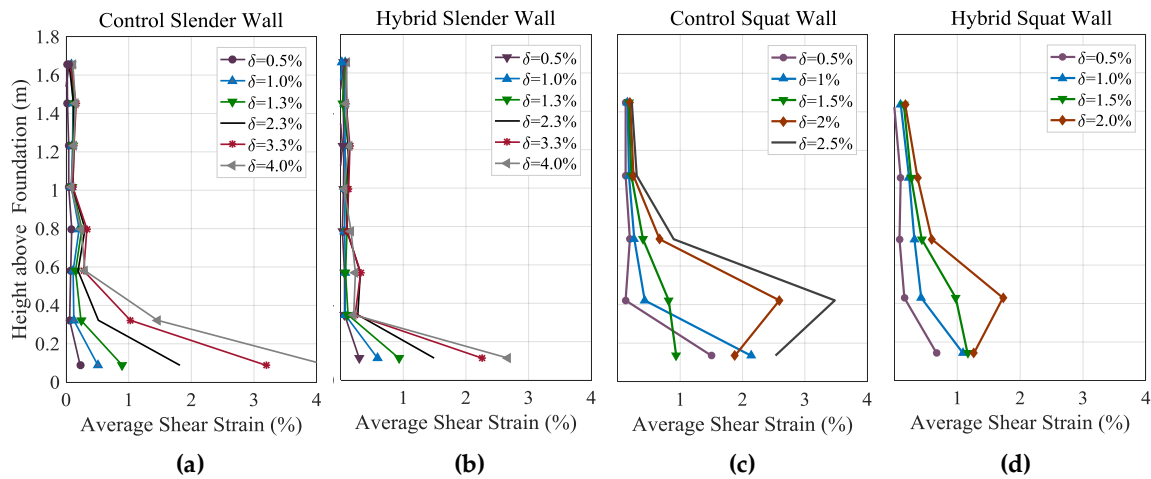


Figure 12. Distribution of average shear strains along the height of each specimen.

The distributions of average shear strains were used to determine the shear components of drift ratios for the specimens, as shown in Figure 13. It can be seen that the control and hybrid squat walls underwent a greater amount of shear drifts in comparison to the control and hybrid slender walls, at equal total drift ratios.

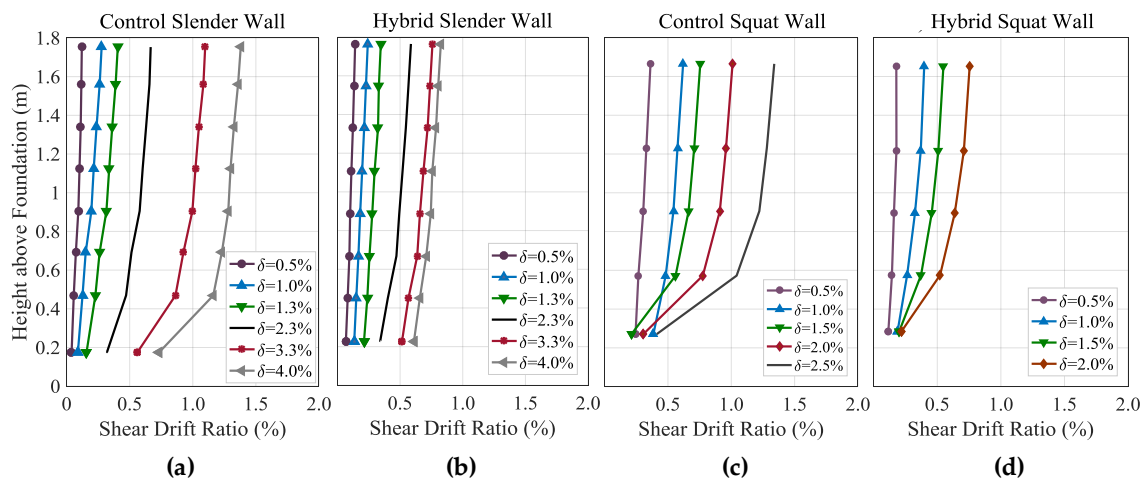


Figure 13. Distribution of shear drift ratios along the height of each specimen.

A similar procedure was used to determine the flexural components of drift ratios for each specimen at different stages of testing. The contribution of flexural and shear drift components at the top point of each wall panel were determined, as illustrated in Figure 14. According to Figure 14, the contributions of flexure and shear in the response of the control slender wall was 82% and 18% at 1.0% drift, and then 80% and 20% at 4.0% drift. The response of the hybrid slender wall was even more influenced by flexure, as it was comprised of 85% flexural and 15% shear deformations at 1.0% drift, and 88% flexural and 12% shear deformations at 4.0% drift.

In the case of squat walls, flexural and shear deformations had equally important contributions to the total response of the specimens. At 1.0% drift, the response of the control squat wall consisted of about 49% flexural and 51% shear deformations. Afterwards, the contribution of flexure in the lateral deformation of the wall decreased to 42% at 2.3% drift, corresponding to 58% contribution of shear deformations. Regarding the hybrid squat wall, flexural and shear deformations were present in 57% and 43% of displacements at 1.0% drift, and 62% and 38% of displacements at 2.1% drift.

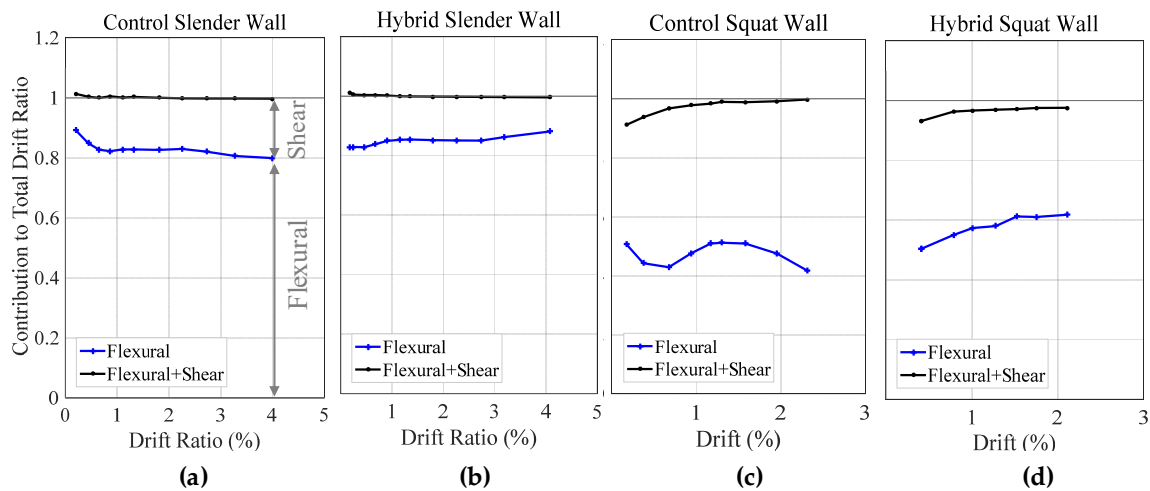


Figure 14. Contribution of flexural and shear deformations in the response of each specimen.

To further investigate the response of the specimens, the ratios of their shear to flexural deformations are shown in Figure 15. It can be seen that the ratio of shear to flexural deformations for the control slender wall was about 0.2 during testing, while it decreased from 0.2 to 0.08. In the case of the hybrid slender wall. For the control squat wall, the ratio of shear to flexural deformations fluctuated between 0.93 and 1.39, while it decreased from 0.85 to 0.57 for the hybrid squat wall.

It is worthwhile to mention that in the GFRP-reinforced shear walls tested by Mohamed et al. [13], shear strains were well distributed over the height of the walls, while the shear strain of the steel-reinforced specimen of the experiment was localized close to its base due to the yielding of its vertical steel bars. In the hybrid walls of this study, the shear strain distribution was affected by the aspect ratios of the walls. The hybrid slender wall behaved similarly to the tested steel-reinforced wall due to the significant yielding of steel bars, while the strain distribution in the hybrid squat wall was distributed more uniformly.

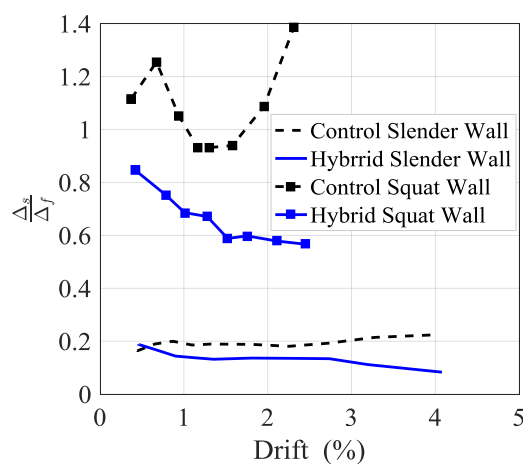


Figure 15. Ratios of shear to flexural deformations of specimens.

The hysteretic response of each shear wall specimen is illustrated in Figure 16. According to Figure 16, each specimen exhibited a symmetric hysteretic response while featuring significant amounts of ductility and energy dissipation. Squat walls had more pinched hysteresis loops as their responses were more influenced by shear deformations in comparison to slender walls. Also, hybrid specimens featured less residual drift ratios in comparison to control walls.

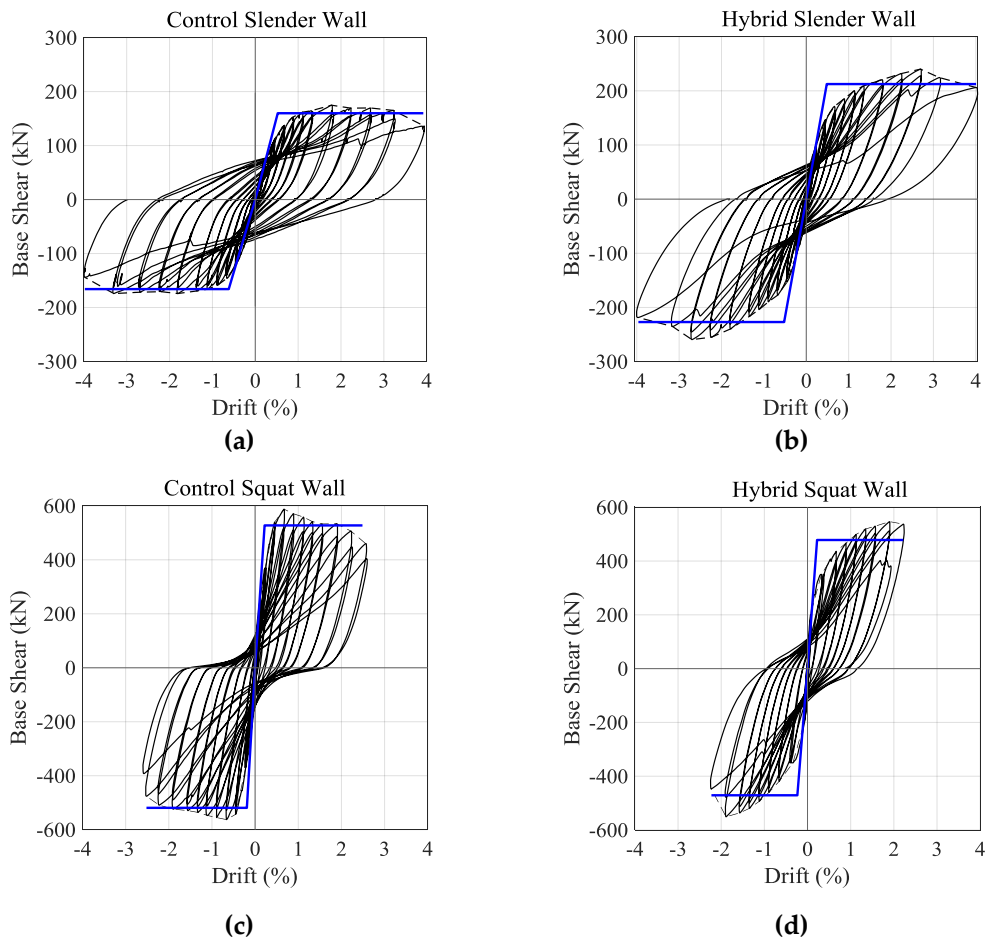


Figure 16. Hysteretic response, backbone curve and idealized backbone of each specimen.

The idealized backbone curve of each specimen was determined based on the equivalent energy elastic-plastic (EEEP) method [14], as shown in Figure 16. The details of idealized response of each specimen are summarized in Table 1. According to Table 1, hybrid walls had comparable yield and ultimate drift ratios, thus comparable ductility indices, compared to the control specimens. In the case of lateral strength and stiffness, the hybrid slender wall reached a greater peak strength than the control slender wall, as it was designed to do. Therefore, the specimen reached greater effective stiffness values. On the other hand, the hybrid squat wall had a comparable yield strength and effective stiffness in comparison to the control squat wall.

Table 1. Specifications of idealized backbone curve of each specimen based on the equivalent energy elastic-plastic (EEEP) method.

Specimen	Yield Drift (%)	Ultimate Drift (%)	Ductility	Yield Strength (kN)	Effective Stiffness (kN/mm)
Control Slender	0.52	3.92	7.3	159.9	15.6
Hybrid Slender	0.48	3.94	8.1	212.5	22.0
Control Squat	0.22	2.49	11.3	527.4	133.2
Hybrid Squat	0.22	2.22	10.0	478.2	120.0

3.3. Self-Centering

Figure 17a,b illustrates the residual drift ratio of specimens during testing. In general, as experiments progressed, and greater drift ratios were applied to the specimens, they sustained more residual drift ratios. However, hybrid shear walls generally exhibited smaller residual drifts than their

corresponding control walls. The reduction in the residual drift ratio of each hybrid specimen with respect to its corresponding control wall is shown in Figure 17c. According to Figure 17c, the maximum self-centering of the hybrid slender wall was observed at -4.0% drift when the residual drift ratio of the specimen was 1.9% , 1.1% smaller than 4.0% the residual drift ratio of the control slender wall. In the case of the hybrid squat wall, maximum reduction in residual drift ratios happened at -2.3% drift with the residual drift ratio of the specimen being -0.96% , 0.35% smaller in amount than -1.31% , the residual drift of the control squat wall.

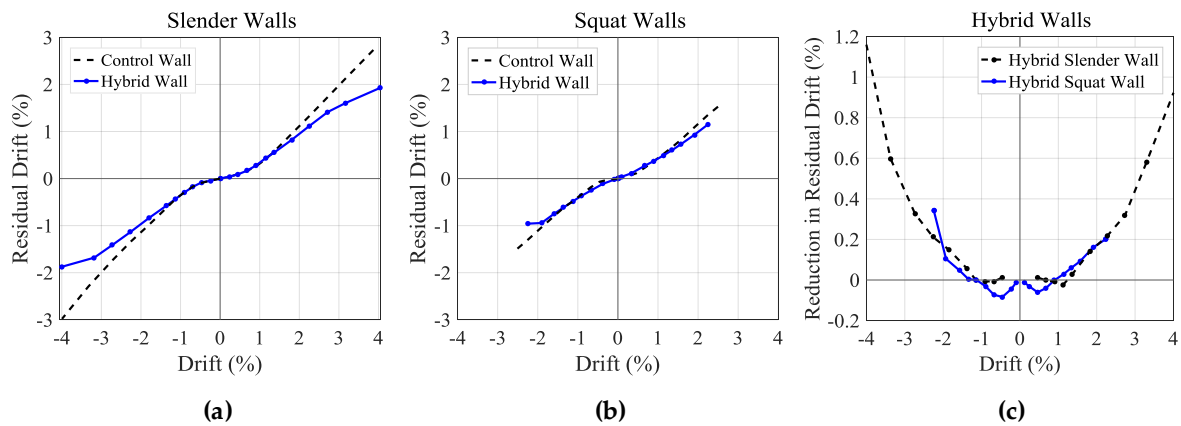


Figure 17. (a) Residual drift ratio of slender walls (b) residual drift ratios squat walls (c) reduction in the residual drift ratios of hybrid walls with respect to control walls.

3.4. Hysteretic Stiffness

Figure 18a,b illustrate peak-to-peak stiffness of specimens during testing. At 0.2% drift, the control and hybrid slender specimens had stiffness values of 20 kN/mm and 25 kN/mm respectively. As the experiments progressed, the stiffness of both specimens decreased, with the hybrid slender wall maintaining a higher stiffness in comparison to the control slender wall. The ultimate stiffness values of the control and hybrid slender walls were 2 kN/mm and 3 kN/mm respectively at 4.0% drift. The control and hybrid squat walls had stiffness values of 91 kN/mm and 93 kN/mm respectively at 0.2% drift. Then, the stiffness of the specimens sharply decreased as the walls started to form cracks and experience yielding. The ultimate stiffness of the control and the hybrid squat specimens were 13 kN/mm and 12 kN/mm respectively at a 2.3% drift.

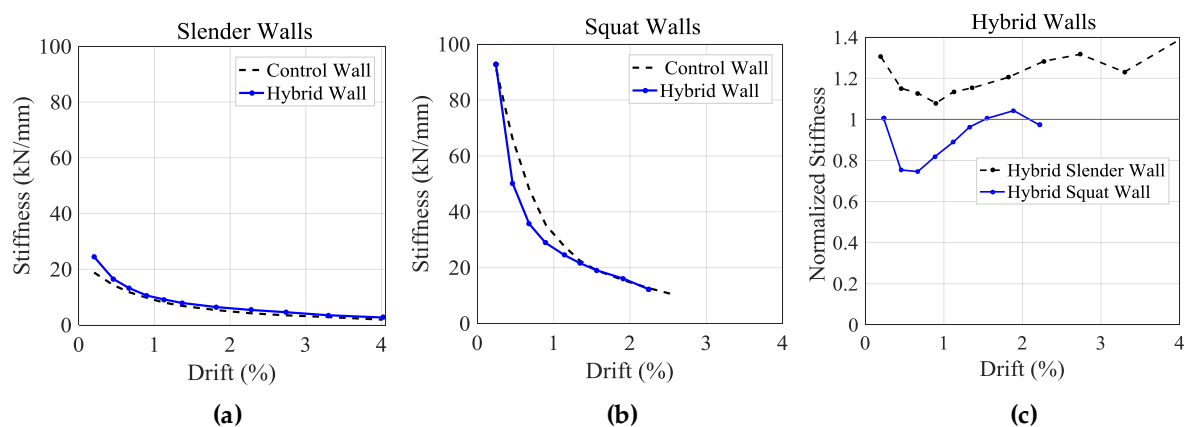


Figure 18. (a) Peak-to-peak stiffness of slender walls; (b) peak-to-peak stiffness of squat walls; (c) normalized peak-to-peak stiffness of hybrid walls.

The ratio of the stiffness of each hybrid wall over that of its corresponding control wall is illustrated in Figure 18c. According to Figure 18c, the stiffness of the hybrid slender wall was between 1.08 and

1.40 of the stiffness of the control slender wall. Also, the stiffness of the hybrid squat wall changed between 0.75 and 1.05 of that of the control squat wall.

3.5. Hysteretic Energy Dissipation

As shown in Figure 19a,b, normalized dissipated energy [15] was used to compare the capacity of specimens to dissipate energy, since they had different levels of lateral strength. As can be seen in Figure 19, for drifts of 1.0% and greater, the hybrid slender and squat walls showed less energy dissipation capacities in comparison to their corresponding control walls.

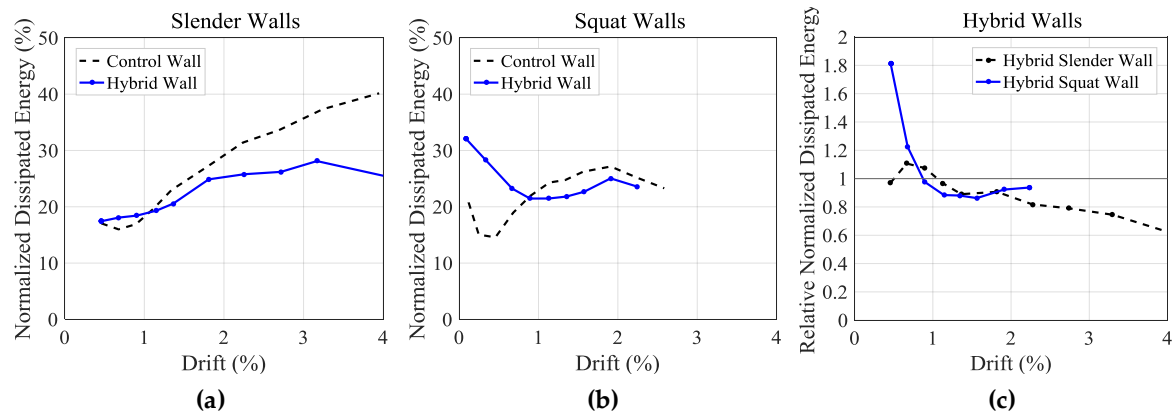


Figure 19. Normalized dissipated energy of (a) slender walls; (b) squat walls; (c) each hybrid wall relative to that of its control wall.

Figure 19c illustrates the normalized dissipated energy of each hybrid specimen over that of its corresponding control wall. According to Figure 19c, the normalized dissipated energy of the hybrid slender specimen changed between 1.11 and 0.62 of that of the control slender wall. In the case of the hybrid squat wall it changed between 0.86 and 1.81 of that of the control squat wall.

4. Discussions

The following conclusions were drawn from this study on the behavior of two hybrid shear walls detailed with steel and GFRP bars and casted with FRCC.

1. The responses of the slender walls were more influenced by flexure than shear, as flexural deformations contributed to about 80% of lateral displacements of the slender walls, while they were responsible for 42% to 62% of the displacements affecting the squat walls. For this reason, it can be concluded that detailing RC shear walls with vertical GFRP bars is more effective in reducing the residual drift ratios of slender shear walls in comparison to squat shear walls. Regarding squat walls, other preparations should also be considered to decrease the residual shear drift ratios of the walls. Also, detailing slender and squat walls with GFRP bars decreased the shear deformations of the walls with respect to their control specimens.
2. Both hybrid slender and squat specimens had slightly greater residual drift ratios in comparison to their control shear walls at drift ratios of 1.0% and smaller. Then the walls showed lower residual drift ratios than their corresponding control walls for drift ratios greater than 1.0%. For this reason, detailing shear walls with GFRP bars could be more effective in improving the collapse prevention seismic performance of the shear walls, rather than their immediate occupancy levels.
3. Special considerations should be taken into account to provide GFRP-reinforced shear walls with adequate levels of stiffness. In this study, the hybrid squat wall, which had a comparable lateral load capacity to the control squat wall, showed lower stiffness in comparison to the control squat wall after cracking, which can impose some problems on the serviceability of the wall. On the

other hand, the hybrid slender wall, which had a higher strength than the control slender wall, maintained a higher stiffness.

4. Both hybrid shear walls dissipated significant amounts of energy. The hybrid specimens showed greater energy dissipation capacities in comparison to their control walls for drift ratios of 1.0% and smaller, when the walls had greater residual drifts than their control walls. However, as the hybrid walls started to have lower residual drifts than their control walls, the energy dissipation capacities of the walls dropped below those of their control walls.
5. The hybrid shear walls displayed comparable ductility indices in comparison to their corresponding control walls. Also, the failures of the hybrid walls were triggered by the failure of their outmost steel rebars, meaning that brittle GFRP bars were well protected in the webs of the hybrid walls.
6. Due to the fiber reinforcement of the hybrid specimens, the walls sustained mitigated damage in comparison to their control walls. In effect, the hybrid walls sustained less cover spalling and fewer concrete cracks.
7. Future studies can focus on the development of valid analytical and finite-element models based on the available experimental data.

Author Contributions: Conceptualization—C.A.C.N.; Data curation—M.J.T.K.; Formal analysis—M.J.T.K.; Funding acquisition—C.A.C.N.; Resources—M.J.T.K., S.G. and C.A.C.N.; Software—M.J.T.K.; Supervision—C.A.C.N.; Writing original draft—M.J.T.K.

Funding: This research was funded by the Natural Sciences Research Council of Canada through its Discovery and Engage Grant programs.

Acknowledgments: The authors thank LafargeHolcim, BP Composites Ltd., McNish Steel and Harris Steel for providing in-kind support for this project.

Conflicts of Interest: The authors declare no conflict of interest.

References

1. Wu, Y.; Liu, T.; Oehlers, D.J. Fundamental principles that govern retrofitting of reinforced concrete columns by steel and FRP jacketing. *Adv. Str. Eng.* **2006**, *9*, 507–533. [[CrossRef](#)]
2. Mohamed, H.M.; Afifi, M.Z.; Benmokrane, B. Performance evaluation of concrete columns reinforced longitudinally with FRP bars and confined with FRP hoops and spirals under axial load. *J. Bridge Eng.* **2014**, *19*, 1–12. [[CrossRef](#)]
3. Mohamed, N.; Farghaly, A.; Benmokrane, B.; Neale, K.W. Experimental investigation of concrete shear walls reinforced with glass fiber-reinforced bars under lateral cyclic loading. *J. Compos. Constr.* **2014**, *18*, 1–10. [[CrossRef](#)]
4. Ghazizadeh, S.; Cruz-Noguez, C.A. Damage-resistant reinforced concrete low-rise walls with hybrid GFRP-steel reinforcement and steel fibers. *J. Compos. Constr.* **2018**, *22*, 04018002. [[CrossRef](#)]
5. Ghazizadeh, S.; Cruz-Noguez, C.A.; Talaei, F. Analytical model for hybrid FRP-steel reinforced shear walls. *Eng. Str.* **2018**, *156*, 556–566. [[CrossRef](#)]
6. Cai, Z.K.; Daiyu, W.; Zhenyu, W. Full-scale seismic testing of concrete building columns reinforced with both steel and CFRP bars. *Compos. Str.* **2017**, *178*, 195–209. [[CrossRef](#)]
7. Parra-Montesinos, G.J.; Kim, K.Y. Seismic behavior of low-rise walls constructed with strain-hardening fiber reinforced cement composites. In Proceedings of the 13th World Conference on Earthquake Engineering, Vancouver, BC, Canada, 1–6 August 2004.
8. American Society of Testing Materials (ASTM). Standard Test Methods and Definitions for Mechanical Testing of Steel Products, ASTM A370-14. Available online: <https://www.scribd.com/document/342633217/A370-14-Standard-Test-Methods-and-Definitions-for-Mechanical-Testing-of-Steel-Products> (accessed on 14 August 2018).
9. American Society of Testing Materials (ASTM). Standard Test Method for Compressive Strength of Cylindrical Concrete Specimens, ASTM C39/C39M-15a. Available online: <http://www.c-s-h.ir/wp-content/uploads/2015/01/C-39.pdf> (accessed on 14 August 2018).

10. Canadian Standards Association (CSA). Design of Concrete Structures, CSA A23.3-14. Available online: https://store.csagroup.org/ccrz__ProductDetails?viewState=DetailView&cartID=&sku=A23.3-14 (accessed on 14 August 2018).
11. Canadian Standards Association (CSA). Design and Construction of Building Structures with Fibre-Reinforced Polymers, CSA S806–S12. Available online: <http://www.iccturkey.com/assets/images/can.csa.s806-02.pdf> (accessed on 14 August 2018).
12. Oesterle, R.G.; Fiorato, A.E.; Johal, L.S.; Carpenter, J.E.; Russell, H.G.; Corley, W.G. *Earthquake-Resistant Structural Walls-Test of Isolated Walls*; National Science Foundation: Washington, WA, USA, 1976.
13. Mohamed, N.; Farghaly, A.S.; Benmokrane, B.; Neale, K.W. Drift capacity design of shear walls reinforced with glass fiber-reinforced polymer bars. *Struct. J.* **2014**, *111*, 1397–1406. [[CrossRef](#)]
14. Park, R. Ductility evaluation from laboratory and analytical testing. In Proceedings of the 9th World Conference on Earthquake Engineering, Tokyo-Kyoto, Japan, 2–9 August 1988.
15. Hidalgo, P.A.; Ledezma, C.A.; Jordan, R.M. Seismic behavior of squat reinforced concrete shear walls. *Earthq. Spectra* **2002**, *18*, 287–308. [[CrossRef](#)]



© 2018 by the authors. Licensee MDPI, Basel, Switzerland. This article is an open access article distributed under the terms and conditions of the Creative Commons Attribution (CC BY) license (<http://creativecommons.org/licenses/by/4.0/>).